International Journal of Engineering Trends and Technology
ISSN: 2231-5381/ https://doi.org/10.14445/22315381/IJETT-V74I5P123

Volume 74 Issue 5, 342-361, May 2026

Original Article

Gram-Charlier Series for Enhanced Areal Roughness Assessment in End-Milled Low-Carbon Steel Surface Replication

Kanaa Thomas[1,2,*], Ngongang Ludovic[1,2], Huisken Mejouyo Paul William[1], Pesdjock Mathieu Jean Pierre[3], Ndongue Esseme Emmanuel[1], Tonye Emmanuel[4]

[1,2]*Department of Mechanical Engineering, Higher Technical Teacher's Training College, University of Douala, P. O. Box 1872, Douala, Cameroon.*
[3]*Cameroonian Association for Research and Innovation in Energy, Technology and Environment, Ebolowa, P.O. Box 59 Ebolowa, Cameroon.*
[4]*Department of Electrical and Telecommunications Engineering, National Advanced School of Engineering of Yaoundé, University of Yaoundé 1, P.O. Box 8390, Yaoundé, Cameroon.*

[*]*Corresponding Author : t_kanaa@yahoo.fr*

Received: 19 January 2026 Revised:19 February 2026 Accepted: 28 March 2026 Published: 30 May 2026

Abstract *- Areal roughness significantly determines surface functionality. Traditional contact methods, though standard, are limiting surface evaluation to single profiles, rendering that evaluation inadequate for multi-tooth processes like milling. Non-contact techniques, however, rely on contact-based regression. This study proposes a framework that applies Gram-Charlier Probability Density Functions (PDFs) to enhance contact measurement accuracy for optimizing surface replication in machining operations. The approach models areal roughness using both Gaussian and Gram-Charlier PDFs. Analysis of 170 milled surfaces under varied machining conditions involves three-dimensional contact measurements that employ Hermite polynomials and cumulants for Gram-Charlier functions construction. The methodology determines roughness values through PDF peak analysis. The methodology determines roughness values through PDF peak analysis. Validation demonstrates that Gram-Charlier models achieve R^2 values exceeding 0.99 across all extraction densities (four to twenty-one linear extractions per surface), confirming superior performance. Response Surface Methodology links this statistical model to machining parameters, enabling replication similarity assessment. Application of Minkowski and Shannon's entropy family distance metrics identifies optimal combinations of spindle speed, depth of cut, and feed per tooth, revealing the depth of cut as the most sensitive parameter, and the carbon steel with 0.15% as the best material over the three selected for achieving precise surface replication control.*

Keywords *- Contact Area Roughness, Gram-Charlier Series, Replicate Surfaces, Similarity/Distance, Response Surface Methodology.*

1. Introduction

The performance of the functional surfaces in mechanisms is significantly influenced by their roughness. Machining and monitoring these surfaces requires strong practical expertise to guarantee optimal performance. Thus, the efficacy of the combined cutting conditions is validated by evaluating the surface parameters post-machining [1, 2]. While defining the surface microtopography accurately, the areal roughness helps to understand its distinction from the profile roughness [3, 4]. The major challenge with the areal roughness assessment resides in the randomness of the surface texture, mostly in non-deterministic surfaces [5, 6]. The milling process, among other machining operations, leads to the production of irregular surfaces at the micro-scale [7]. This is fundamentally due, for most milling operations, to the passage of multiple cutting teeth of the tool to produce the same surface [8], as well as the occurrence of surface-cutting phenomena like chattering [9].

Measuring the surface texture with a probe (stylus) has been declared faithful regarding the norms surrounding the method. It is, however, considered time-consuming when attempting to measure at different points on the same surface for assessing the areal roughness [10-12]. Despite the accuracy of modern/optical topography measurement instruments, the optical areal roughness assessment still asks for deep computing and light explanations, to be well understood. The complexity of the control or measurement methods of the real surface roughness has been highlighted by the works of several authors [13-17]. The irregularity of the

profile from the same surface induces a variation of the linear roughness values taken with a probe at different points. This highlights the importance and the difficulty of determining the contact area roughness. [18] defined a random variable as a variable that can take on a finite number of distinct values.

A random variable can be understood with its distribution law, which is articulated mathematically through the distribution function derived from the first and second characteristic functions, identified as the moments and cumulants, respectively [19]. Thus, linear roughness can be considered as a random variable whose behavior has to be determined by a Probability Distribution Function (PDF). In the process of modeling random events (with normal distribution, Poisson distribution, Weibull distribution, etc.), the normal distribution is a prominent choice, distinguished by its key parameters: mean and standard deviation. The most popular technique used for highlighting the global behavior of random variables in systems is the optimization of the Probability Density Function [20, 21].

Over the years, developments of the Gaussian distribution with two variables, the asymptotic expansion of the normal distribution, the Mac Laurin series, and the Gram-Charlier series have all contributed to the estimation of the characteristic functions [22-25] needed to appreciate the local spreading/concentration of values of a variable in experimentation. Some works have notably formulated the surface modeling with statistical methods, and some others have reviewed several approaches related to that modeling [26, 27, 28]. The significance of the Gram-Charlier series cannot be overstated, as it effectively transforms the probability density function into a summation of reduced centered polynomials. This series proves particularly valuable for modeling distributions that deviate from normality or are not easily described by their moments. Furthermore, Gram-Charlier (orthogonal series) presents a compelling alternative for estimating the Probability Density Function in comparison to a normal density [22].

Mostly used in the domain of Finance for its flexibility in the variable's fluctuation, the Gram-Charlier series was employed in [29]'s work on portraying the expansion as a density. The findings suggest that including skewness and kurtosis as parameters in the Gram-Charlier expansion makes the series a widely favored choice in Finance. [30] improved Gram-Charlier expansion by choosing new values of the Gaussian parameters. The reproducibility of the PDF and the evaluation of the input moments are then improved. [31] Rather, we used Gram-Charlier expansion in a multivariate series of given distributions in self-orthogonal polynomials to adjust the moments of interest. Modifying the kurtosis helped to better model the PDF in empirical conditions and to compute risk measures like Value at Risk and the Expected Shortfall. By applying Gallant and Nychka's (1987) method to the study of Jondeau and Rockinger (2001), [32] extended the Gram-Charlier density properties to investigate parametric properties. This led to obtaining analytical kth-order stationarity of moments based on a modified approach to Gram-Charlier under unimodality conditions.

Several additional domains have implemented the Gram-Charlier series to improve the optimization of the probability density functions. In the Engineering field, [33] formulated a Gram-Charlier series to express non-normal densities as infinite series involving the normal density and its derivatives. They optimized the parameters of the normal distribution to improve the method and facilitate the reproducibility of the probability density function. [34] compared the performance of the Weibull and Gram-Charlier distributions to low-occurrence strong wind speed distributions of idealized structures under different conditions. The development of the Gram-Charlier series up to the 6th term provides greater flexibility for the method and greater accuracy in certain areas. [35] experimented with the simulation of batch precipitation of silica with a mathematical approach involving statistical moments. The Gram-Charlier expansion allowed the reconstruction of the particle size distribution, leading to pinpointing key values of the density function.

Some works are nuancing the use of the Gaussian distribution over the Gram-Charlier series, and taking into consideration the wider use of this previous in experimentation as well as its attractive alternative in estimating the Probability Density Function of a random variable [22, 36-38]. Traditional areal roughness methods assume Gaussian distributions or rely on the mean values of parameters without probabilistic validation [28]. Recent measurement system analysis frameworks quantify instrument uncertainty like bias and repeatability, but do not model surface characteristic distributions across replicates, limiting process repeatability assessment.

When a random variable is sampled from a particular distribution, it is possible to assess the distance/similarity between this variable and another variable originating from a different distribution. To derive meaningful insights from such comparisons, the distributions must be formulated within a coherent framework [39-42]. The practice of statistics involves data manipulation, and once valuable datasets are established, it is essential to perform analyses, particularly in the context of comparing datasets for similarities. Thus, identifying suitable tools for data similarity analysis requires an understanding of their practical applications and the interpretation of the significance of their results. Several methods focus on distance metrics for similarity measurement, but their implementation is frequently influenced by the types of data being examined. Some authors have provided significant coverage of the techniques in paper review, and many researchers have utilized distinct similarity distance metrics to tackle specific challenges.

In their works, [43] examine the use of distance metrics in similarity estimation and find that popular metrics like Euclidean and Manhattan distance may not be suitable for all data distributions. They proposed a new guideline to relate distribution models to similarity estimation and new distance metrics. In 2007, [44] systematically identified and classified the distance and similarity measures applicable to Probability Density Functions across different families, emphasizing both syntactic and semantic connections. While presenting the most used techniques, the research highlighted six (06) approaches that are notably lacking in the existing literature and warrant further investigation. The research conducted by [45] focused on the comparative analysis of measurements applied to binary and numerical datasets, employing tools related to similarity, distance, and scalar products.

By formulating an equivalence scale grounded on the generalized Kendall [38] coefficient, they demonstrated that the stability characteristics of comparison measurements, as well as the variations in the equivalence scale, are influenced by the inherent nature of the data. [46] undertook an extensive examination of seventy-six (76) similarity and distance measures utilized throughout the last century for hierarchical clustering classification. Their analysis revealed three primary groups: distance-based measures, non-correlation measures, and correlation-based measures. [47] proposed a guide for researchers that examines fourteen (14) different similarity metrics. After defining the data's nature, followed by an exploration of feature selection methodologies, the authors then presented formulas for measuring similarities and differences. They ultimately provided a comparative analysis of the complexity, strengths, and weaknesses of the metrics, as depicted in a multiclass similarity measurement table.

[48] employed Chebyshev distance for the classification of radar images. They introduced a divergence-Chebyshev distance metric to represent the similarity between pixels in the images under comparison. Their findings demonstrated that the classifier utilizing this specific distance parameter outperformed alternative classification methods.

Employing the Probability Density Function (PDF) with a normal Gaussian approach has produced, under specific conditions, interesting results in several fields, namely Finance, engineering, machine learning, speech processing, and medical imaging [49-53].

The optimization of the PDF with the higher-order moments established by the Gram-Charlier series is introduced for both Gaussian and non-Gaussian deviations as a thought-provoking method to characterize random phenomena [54, 55]. An insight is then raised in conducting a comparative study of results obtained from both experimental methods in their identification of the most reliable approach, especially concerning its use in the repeatability of the conditions and parameters that generate the estimated quantity.

This work addresses gaps in areal roughness assessment through three main points, namely applied probabilistic characterization, quantitative replication metrics, and process optimization. Firstly, higher-order statistical moments will be applied at a significant-order Gram-Charlier expansion to linear roughness measurements. Secondly, four metric distances will be implemented for machined surface similarity assessment. Thirdly, Response Surface Methodology, integrating roughness distributions with machining parameters, will be used to identify optimal replication conditions.

This paper is organized into four sections. Section 2 will present the materials used to create the database and the methods employed to process the data to achieve the objectives. Section 3 will highlight the results and position the work in the literature. Section 4 will summarize the findings and open the perspectives related.

2. Materials and Methods

2.1. Materials

The spectrometer Foundry Master, Oxford Instruments Analytical Gmbh® helped to determine the materials' chemical composition (Table 1).

Table 1. Average values of the tests of the chemical composition of the samples

Sample	Number of tests	Iron, (Fe)	Carbon (C)	Silicon (Si)	Phosphorus (P)
01	2	99.3	0.05	0.03	0.05
02	2	96.6	0.32	0.25	0.03
03	2	98.7	0.14	0.04	0.04
Sample	Number of tests	Sulfur (S)	Chromium (Cr)	Molybdenum (Mo)	
01	2	0.01	0.03	0.007	
02	2	0.05	0.17	0.031	
03	2	0.04	0.15	0.011	

Based on the chemical composition from the tests, the samples were identified as AISI1010, AISI1017, and AISI1038. A milling machine, Milko35r, and the cutting tool BAP400R-63-22, Face milling cutter with 4 inserts Apkt 1604pdr-m, grade U9145, were used to produce surface samples. The MarSurf PS10® roughness tester with probe

measured the linear roughness values on the surface samples. The Intel® CoreTM i7-8550-CPU @1.80GHz-1.99GHz with 12GB of RAM and the software Visual Studio Code V1.91.0® served for the data processing environment to estimate the areal roughness.

2.2. Methods

2.2.1. Surface Samples Creation

The creation of the surface samples (also called finite surface samples, $\mathcal{F}_s$It was organized around the milling process.

Variations were carried out at three levels for the spindle speed (N in rpm), the feed per tooth (f or f_z in mm/tooth), and the depth of cut (DoC in mm) and the carbon content (Table 2). The recording process of the tool life (Tl in s) was carried out after each experience.

Table 2. Level of machining conditions for the surface samples

Level	Carbon content (wt%)	Depth of cut (mm)	Spindle speed (rpm)	Feed per tooth (mm/tooth)
-1	0.1	0.1	910	0.016
0	0.15	0.2	1095	0.0225
+1	0.3	0.3	1280	0.029

After considering a full factorial design, to evaluate variable effects and improve estimation precision, which explores all the distinct combinations ($D_c = l^k$) of k-factors at l-levels ($k = 4, l = 3$), an alternating replication strategy was implemented. It is based on the law of large numbers, which establishes empirical mean convergence to expectation. Single replication per surface specimen (Figure 1) reduces variance by 50% [56]. Center-point replicates (0, 0, 0, 0) permit the pure error estimation and $n_0 = 4$ was chosen to provide 3 degrees of freedom.

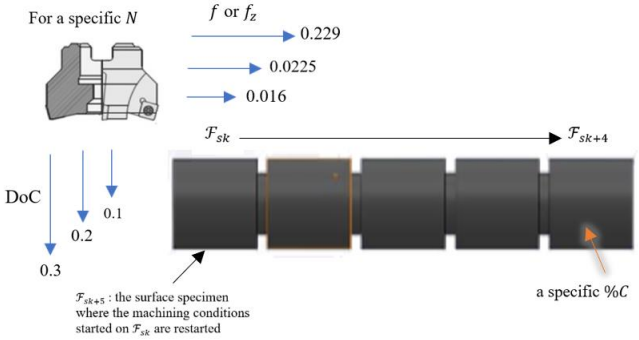

Fig. 1 Surface specimen and replicates creation principle

The total number of experiments n_{exp} was organized into blocks of five consecutive experiments followed by their 5 respective replications (Figure 1), repeating until all Distinct Combinations (D_c) are exhausted, and the consideration related to the center-point replicates.

$$n_{exp} = 2 \times (D_c + n_0)$$
$$= 2 \times (81 + 4) = 170 \text{ experiments}$$

2.2.2. Areal roughness determination

The Gram-Charlier series expands the probability density to which the Hermite polynomials are included. It therefore permits us to appreciate, with extracted data, the non-Gaussian roughness distribution. Hence, let $\mathcal{F}_{sk}$ be the k-th finite surface under measurement. It is defined $r_l^{(i)}$as the i-th linear roughness, where $\in \{1, 2, \dots, N_p\}$, N_p as the total number of linear profile measurements taken on $\mathcal{F}_{sk}$, and P_v as the fixed pitch distance between consecutive measurement positions. $\mathcal{F}_s$ produces two different sets (Equation (1)). The first $\mathcal{R}$ is the set of profile measurements taken over the surface, and the second r_l (a random variable) as the set of parameters measured by the probe during its displacement in $r_l^{(i)}$ Moreover, values related to each parameter.

$$\mathcal{R} = \{r_l^{(1)}, r_l^{(2)}, \dots, r_l^{(N_p)}\};$$
$$r_l = \{r_a/R_a;\ r_z/R_z;\ r_q/R_q; \dots\}$$
$$\text{with } r_a = \{r_a^{(i)}; i \in \mathbb{N}^*\} \quad (1)$$

It is assumed that the standard deviation of the unimodal distribution of linear roughness (r_lThe values from the surface sample are identical to the Gaussian distribution of the Gram-Charlier series [22,30]. However, modeling the probability density function by the Gaussian distribution is one of the most commonly used distributions for modeling random phenomena. It is characterized by the mean and standard deviation. It is therefore not going to be highlighted here, but rather its extension to Gram-Charlier development and the results from its application will be presented.

$D(r_l)$ is then defined as the Probability Density Function (PDF) of linear roughness with Gram-Charlier series, expressed in terms of the cumulants Q_p, the Hermite polynomials H_p of order p [37] and the Gaussian function (kernel) $f(r_l;\ \alpha, \beta) = \frac{1}{\beta\sqrt{2\pi}} e^{-\frac{(r_l-\alpha)^2}{2\beta^2}}$ containing the variable r_l, the mean α and the standard deviation β.

$$D(r_l) = f(r_l; \alpha, \beta)\left[Q_0 H_0 + \sum_{p=0}^{\infty} Q_p H_p\left(\frac{r_l-\alpha}{\beta}\right)\right] \quad (2)$$

With $Q_0 = 1, H_0(r_l) = 1$.

For an experimental approach to reduce the calculations [55, 57], data have been normalized so that $\alpha = 0, \beta = 1$.

$$\mathfrak{s}_i = \frac{r_l^{(i)} - \hat{\alpha}}{\hat{\beta}} / \ \hat{\alpha} = \frac{1}{N_P}\sum_{i=1}^{N_P} r_l^{(i)}$$

and $\hat{\beta}^2 = \frac{1}{N_P - 1}\sum_{i=1}^{N_P}(r_l^{(i)} - \hat{\alpha})^2$

With $\hat{\alpha}, \hat{\beta}$ as the respective sample mean and standard deviation.

From a mathematical perspective, for any $p \in \mathbb{N}_+$,

$$H_p(\mathfrak{s}) = (-1)^p e^{(\mathfrak{s})^2} \frac{d^p}{d\mathfrak{s}^p} e^{-(\mathfrak{s})^2} \quad (3)$$

Thus, a simpler expression of $D(r_l)$ becomes $D(\mathfrak{s}) = f(\mathfrak{s}) . \sum_{p=0}^{N} \hat{Q}_p H_p(r_l)$ with $\hat{Q}_p \neq 0$ and $\mathrm{N} \in \{2p,\ p \in \mathbb{N}^+\}$ in order to substitute (2) and (3)We obtained the following

$$D(\mathfrak{s}) = f(\mathfrak{s}; 0, 1) . \sum_{p=0}^{N} \hat{Q}_p . (-1)^p e^{(\mathfrak{s})^2} \frac{d^p}{d\mathfrak{s}^p} e^{-(\mathfrak{s})^2}$$

Fully dependent on p-order statistical moments, the cumulants $\hat{Q}_p$ are estimated by considering the orthogonality property of Hermite polynomials. Thus, for any $j \in \mathbb{N}_+$,

$$\begin{aligned} \int_{-\infty}^{+\infty} H_j(\mathfrak{s}) . D(\mathfrak{s}) d\mathfrak{s} &= \int_{-\infty}^{+\infty} H_j(\mathfrak{s}) \left[f(\mathfrak{s}) \sum_{p=0}^{+\infty} Q_p . H_p(\mathfrak{s}) \right] d\mathfrak{s} \\ &= \sum_{p=0}^{+\infty} Q_p . \int_{-\infty}^{+\infty} H_j(\mathfrak{s}) H_p(\mathfrak{s}) f(\mathfrak{s}) d\mathfrak{s} \\ &= Q_j . j! \end{aligned} \quad (4)$$

By orthogonality: $\int_{-\infty}^{+\infty} H_j H_p f(\mathfrak{s}) d\mathfrak{s} = \delta_{\{jp\}} . p!$

Thus, the sample cumulants are given by Equation (5).

$$\hat{Q}_p = \frac{1}{p!} \sum_{k=0}^{[p/2]} \frac{(-1)^k p!}{k!(p-2k)!2^k} \mu'_{p-2k} \quad (5)$$

with μ'_p: the p-th sample moment, also known as the mathematical expectation value / $\mu'_p = \frac{1}{N_p} \sum_{i=1}^{N_p} \mathfrak{s}_i^p$, calculated as in [55, 58]. Hermite polynomials are derived using the recursive formula Equation (6) for any $n \geq 1$, and $H_0(\mathfrak{s}) = 1$,

$$H_{n+1}(\mathfrak{s}) = \mathfrak{s} . H_n(\mathfrak{s}) - n . H_{n-1}(\mathfrak{s}) \quad (6)$$

with $H_0(\mathfrak{s}) = 1, \quad H_1(\mathfrak{s}) = \mathfrak{s}$

The multiplier coefficient of the orthogonal polynomials is recognized to be invariant for the degree at which the series is truncated [59]. From the assumption stated above, the conditions in which Gram-Charlier series are positive and unimodal [60-62], and the developments of the Equations (3) and (4) as in [30], the development of the distribution function here is stopped in a suitable number of terms (7), with the investigations being conducted through empirical methods.

$$\begin{aligned} D(\mathfrak{s}) = f(\mathfrak{s}) . \big[&\hat{Q}_0 H_0(\mathfrak{s}) + \hat{Q}_1 H_1(\mathfrak{s}) + \hat{Q}_2 H_2(\mathfrak{s}) + \\ &\hat{Q}_3 H_3(\mathfrak{s}) + \hat{Q}_4 H_4(\mathfrak{s}) \big] \end{aligned} \quad (7)$$

With $\hat{Q}_0 = 1, \hat{Q}_1 = 0, \hat{Q}_2 = 0, \hat{Q}_3 = \frac{\mu'_3}{6}, \hat{Q}_4 = \frac{\mu'_4 - 3}{24}$

For the formulation of the areal roughness, based on the distribution function, it is considered a finite surface (surface sample) $\mathcal{F}_{sk}$ with N_p of r_l measurements respecting the edge conditions established by [63]. This configuration (Figure 2) is essential to avoid the interference of the stylus tip groove-prints demonstrated by [10].

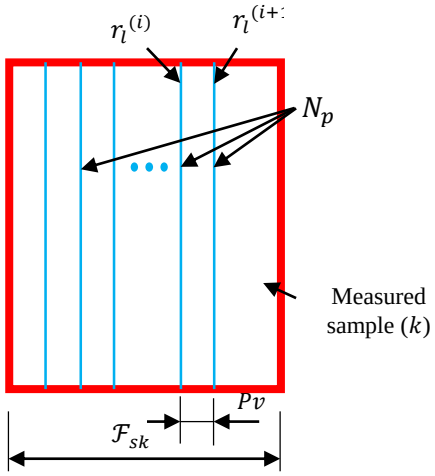

Fig. 2 3-D extraction of linear roughness (r_l) values

The areal roughness of a finite surface $R_s(\mathcal{F}_{sk})$ is then defined as the roughness value around which the surface exhibits the highest probability density of $D(z)$ as stated in Equation (8).

$$R_s(\mathcal{F}_{sk}) = \hat{\alpha} + \hat{\beta} . \hat{z}_H$$

$$\hat{z}_H = \arg\max_z D(z) \Leftrightarrow \left. \frac{dD(z)}{dz} \right|_{z=\hat{z}_H} = 0$$

$$\text{And} \quad \left. \frac{d^2 D(z)}{dz^2} \right|_{z=\hat{z}_H} < 0 \quad (8)$$

$\hat{z}_H$ Here represents the most probable standardized roughness value.

2.2.3. Experimental validation and statistical significance

The effectiveness of the Gram-Charlier-based areal roughness is validated by examining its convergence behavior as a function of the number of measurements. N_p. And so, for a number of surface samples $\{\mathcal{F}_{s1}, \mathcal{F}_{s2}, \dots, \mathcal{F}_{sN}\}$It is performed for each sample δ linear roughness measurements.

For each $N_p \in \langle 4, 5, \dots, \delta \rangle$ it is randomly selected N_p measurements from the available δ measurements. $R_s^{(N_p)}(\mathcal{F}_{sk})$ is then computed and compared against the reference $R_s^{(\delta)}(\mathcal{F}_{sk})$. For its generic and bounded performance measure in data [64], the coefficient of determination R-squared (R^2) is used as the criterion to

observe the performance of the areal roughness estimation for both approaches (Equation (9)).

$$R^2(N_p) = 1 - \left(\frac{\sum_{k=1}^{N} \left(R_s^{(\delta)}(\mathcal{F}_{sk}) - R_s^{(Np)}(\mathcal{F}_{sk}) \right)^2}{\sum_{k=1}^{N} \left(R_s^{(\delta)}(\mathcal{F}_{sk}) - \overline{R_s^{(\delta)}} \right)^2} \right) \quad (9)$$

Where $\overline{R_s^{(\delta)}} = \sum_{k=1}^{N} R_s^{(\delta)}(\mathcal{F}_{sk})$ is the mean reference roughness across all samples.

The statistical significance testing is organized around the convergence rate $CR(N_p)$ according to the number of measurements N_p (Equation (10)).

The convergence is validated when $CR(N_p)$ remain below the threshold τ (with τ = 1/100) for three (03) consecutive experiments.

$$CR(N_p) = \left| R^2(N_p) - R^2(N_p - 1) \right| < \tau \quad (10)$$

2.2.4. Distance of the Areal Roughness on Replicate Surfaces

The machined surfaces from the same material, tool life, and under uniform machining conditions (spindle speed, feed rate, and depth of cut) were evaluated for their distance/similarity using Response Surface Methodology with experimental data as advised in the empirical modeling [65]. Ideally, those surfaces should exhibit identical areal roughness characteristics.

The degree of surface repeatability was quantified by measuring how closely areal roughness values matched between replicate surfaces. Lower distance values ($d_{name(N,f,DoC)}$) indicate better process repeatability. Four distance metrics were employed to quantify differences in areal roughness between pair replicate surfaces ($\mathcal{F}_{sk}$ and $\mathcal{F}_{sk+5}$, with k and $k+5$ being their numbering, as shown previously in Figure 1.

These four metrics provide complementary perspectives: in Minkowski's family, Minkowski (Equation (11)) captures overall deviation, Chebyshev (Equation (12)) identifies maximum discrepancy, while in Shannon's entropy family, Kullback-Leibler (Equation (13)) and Jensen-Shannon (Equation (14)) quantify distributional dissimilarity [41].

$$d_{MK(\mathcal{F}_{sk},\mathcal{F}_{sk+5})} = \sqrt[N]{\sum_{N_p=4}^{\delta} \left| R_{s\,(\mathcal{F}_{sk})}^{N_p} - R_{s\,(\mathcal{F}_{sk+5})}^{N_p} \right|^N} \quad (11)$$

$$d_{Cheby(\mathcal{F}_{sk},\mathcal{F}_{sk+5})} = \max_{\delta} \left| R_{s\,(\mathcal{F}_{sk})}^{\delta} - R_{s\,(\mathcal{F}_{sk+5})}^{\delta} \right| \quad (12)$$

$$d_{KL(\mathcal{F}_{sk},\mathcal{F}_{sk+5})} = \sum_{N_p=4}^{\delta} R_{s\,(\mathcal{F}_{sk})}^{N_p} \ln \frac{R_{s\,(\mathcal{F}_{sk})}^{N_p}}{R_{s\,(\mathcal{F}_{sk+5})}^{N_p}} \quad (13)$$

$$d_{JS(\mathcal{F}_{sk},\mathcal{F}_{sk+5})} = \frac{1}{2}\left[\sum_{N_p=4}^{\delta} R_{s\,(\mathcal{F}_{sk})}^{N_p} \ln \left(\frac{2R_{s\,(\mathcal{F}_{sk})}^{N_p}}{R_{s\,(\mathcal{F}_{sk})}^{N_p} + R_{s\,(\mathcal{F}_{sk+5})}^{N_p}} \right) \sum_{N_p=4}^{\delta} R_{s\,(\mathcal{F}_{sk+5})}^{N_p} \right] + \frac{1}{2}\left[\ln \left(\frac{2R_{s\,(FS_{k+5})}^{N_p}}{R_{s\,(FS_k)}^{N_p} + R_{s\,(FS_{k+5})}^{N_p}} \right) \right] \quad (14)$$

2.2.5. Response Surface Modeling

Response Surface Methodology (RSM) was used to model the relationship between machining parameters and surface repeatability.

The goal was to identify parameter combinations that minimize distance metrics $d_{name(N,f,DoC)}$, thereby maximizing process consistency.

For each distance metric, a second-order polynomial regression (Equation (15)) model was fitted:

$$d_{name(N,f,DoC)} = \beta_0 + \beta_1 f + \beta_2 N + \beta_3 DoC + \beta_{11} f^2 + \beta_{22} N^2 + \beta_{33} DoC^2 + \beta_{12} f \cdot N + \beta_{13} f \cdot DoC + \beta_{23} N \cdot DoC + \varepsilon \quad (15)$$

where:

$d_{name(N,f,DoC)}$: distance metric; $\beta_0, \beta_i, \beta_{ii}, \beta_{ij}$: regression coefficients and ε: random error.

The model captures linear effects (β_i), quadratic effects (β_{ii}), and two-way interactions (β_{ij}) between machining parameters. Table 3 summarizes the validation metrics and acceptance criteria used in the works.

Table 3. validation metrics and acceptance criteria used

Statistical Metric	Formula	Acceptance Criterion	Practical Meaning
F-statistic	$F = MS_{Model} / MS_{Error}$	p-value < 0.05	Parameters affect repeatability
R^2	SS_{Model}/SS_{total}	p-value > 0.75	Model explains > 75% of variation
Adjusted R^2	$1 - \left[\frac{(1-R^2)(n-1)}{(n-p-1)}\right]$	p-value > 0.75	Good fit accounting for model complexity
Predicted R^2	1 - $PRESS/SST_{otal}$	Within 0.20 of Adj-R^2	Model predicts new data reliably

3. Results and Discussion

3.1. Results

3.1.1. Dataset of Surface Samples and Roughness Values

The finite surfaces from the same workpiece were separated with grooves to distinguish and reference them (Figure 3) from the same and at opposite faces.

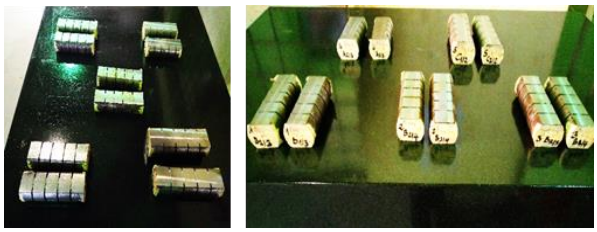

Fig. 3 Surface samples before the database collection (side and front views)

The in-process setup (Figure 4) of the linear roughness extraction helped to create a database of one hundred and seventy (170) finite surfaces for three thousand nine hundred and ten (3910) linear roughness values of Ra extracted.

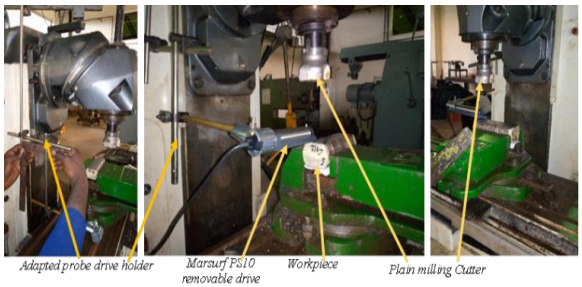

Fig. 4 In-process setup of the 3-D linear roughness r_l extraction on FS_{16}

Table 4 and 5 (start and end) presents a matrix of eighteen experiences from one hundred and seventy machining trials, randomly sampling across the improved full factorial design with replicates (§2.2.1). Some experiences of the selected subset constitute the results that are displayed in the presentation in this section. The surface replication outcomes measured through four distance metrics, from the geometric family (Minkowski and Chebyshev) and the entropy family (Kullback-Leibler and Jensen-Shannon), are calculated from the areal roughness determined at Equation (8).

3.1.2. Areal Roughness Determination

An extraction from a finite surface F_{sk} of linear roughness values with the pitch value $Pv = 1mm$ between $r_{l,j+1}$ and $r_{l,j}$ (two consecutive lining samplings), resulted in obtaining the points belonging to the PDF in the Gaussian and Gram-Charlier distribution functions The connection of the $N_p = 23$ points sampling of $\boldsymbol{r_l}$, driven by the Gaussian function $f(\mathfrak{s}, 0, 1)$ defined (§2.2.3) of N_i values where N_i and N_{i+1} are pitched at 1/10000. The determination of the cumulants and Hermite polynomials allows the plotting of $D(r_l)$ from Gram-Charlier as a function of the N_p values of r_l. Figure 5 presents a comparative visualization of the probability distribution functions (PDFs) linking the experimental values of the arithmetic roughness parameter (r_a) from the values of ${r_a}^i$ measured on surface samples F_{S2}, F_{S16}, F_{S103}. The figure explicitly illustrates the shape discrepancy between these two distributional models, revealing that Gram-Charlier PDFs capture the non-Gaussian characteristics inherent to the additional values (statistical moments) used to build them.

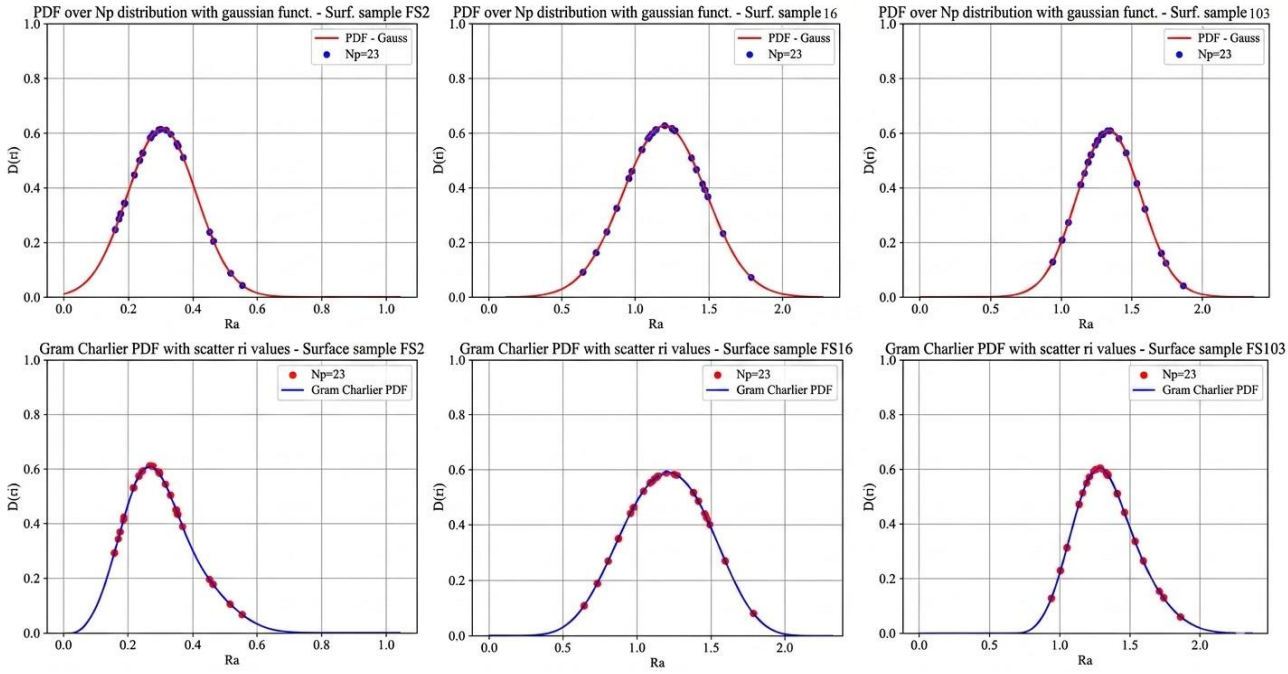

Fig. 5 Distribution function $D(r_l)$ with $N_p = 23$ and r_l values of surface samples F_{S2}, F_{S16}, F_{S103}

A superimposed plotting of the curves for the measurement sets with peak values of the Gram-Charlier PDF over the Gaussians was performed for all the surface samples at different. N_p. Figure 6 displays the upper, for the surface samples. F_{S2}, F_{S16}, F_{S103} with $N_p = 23$, the maximum for each PDF from which the areal roughness is derived, and the areal roughness $R_s(\mathcal{F}_{sk})$ is displayed below each surface sample according to the number of measurements N_p. For the twenty-three (23) measurements of linear roughness Values, Mean, Standard Deviation (*Std Dev*), Skewness, and Kurtosis have been calculated.

The areal roughness $R_{s(FS_k)}$ (Equation (8)) was determined for Gaussian (*Gauss areal*) and Gram-Charlier (*GC areal*) distributions. Table 6 highlights the results for the 18 experiences given in Table 4. There is conformity between the calculated mean and the determined Gaussian areal roughness, validating the PDF connecting the experimental values within the same experience. The areal roughness from the Gram-Charlier distribution function $D(r_l)$ permitted to underline the difference introduced by the statistical moments of higher order. The reliability of the mean and Gaussian roughness across the measurement sets validated the experimental formulation and determination of areal roughness with the distribution functions.

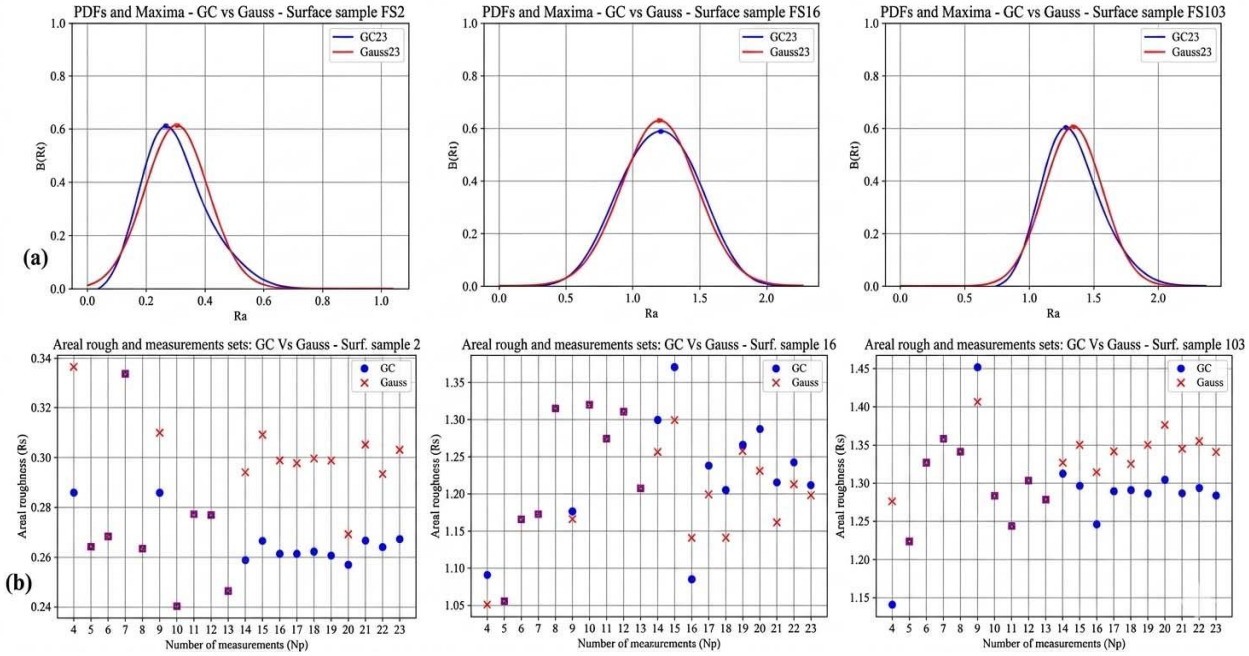

Fig. 6 PDFs, maxima, and areal roughness values with the number of measurements for the samples FS_2, FS_{16} and FS_{103}. (a) Maxima of $D(r_l)$ with GC and Gaussian approaches. (b) Areal roughness values with the number of measurements.

Table 6. Statistical moments and Areal roughness (Gauss and Gram-Charlier)

Exp	Mean	Std Dev	Skewness	Kurtosis	Gauss Areal roughness R_s	GC Areal roughness R_s
FS_1	0.2603	0.0749	1.5625	2.7319	0.2603	0.2410
FS_2	0.303	0.1079	0.7324	- 0.2232	0.303	0.2673
FS_6	0.428	0.1656	- 0.1004	- 1.0732	0.4283	0.461
FS_7	0.5373	0.149	- 0.129	- 1.074	0.5373	0.5519
FS_{10}	0.9693	0.1929	0.5206	0.9868	0.9693	0.9396
FS_{11}	1.337	0.4282	- 0.513	- 0.7461	1.3374	1.4851
FS_{14}	1.7493	0.2969	- 0.2196	- 0.2263	1.7493	1.7861
FS_{15}	1.653	0.2257	0.2157	- 0.6339	1.653	1.6153
FS_{16}	1.6237	0.1478	- 0.1007	- 0.8431	1.6237	1.639
FS_{18}	1.6453	0.2289	- 0.2442	- 1.0307	1.645	1.7072
FS_{19}	1.6433	0.2047	- 0.468	- 0.2918	1.6433	1.6942
FS_{46}	0.447	0.1114	1.563	2.007	0.447	0.4138
FS_{47}	0.4321	0.1795	1.2323	0.499	0.4321	0.3678
FS_{92}	1.1835	0.1224	- 0.0839	- 0.9308	1.184	1.195

$\mathbf{FS_{100}}$	1.4136	0.4052	2.4367	0.6049	1.4136	1.3188
$\mathbf{FS_{141}}$	1.7403	0.2073	1.2571	0.9463	1.7403	1.6735
$\mathbf{FS_{161}}$	1.466	0.1727	- 0.4021	0.8956	1.4667	1.4883
$\mathbf{FS_{169}}$	1.734	0.2745	0.7815	2.1035	1.734	1.681

3.1.3. Gram-Charlier areal Roughness versus Gauss Areal Roughness

As illustrated in Figure 7, the areal roughness values exhibit a strong clustering ($R^2 \geq 0.96$) across four (04) to twenty-one (21) measurements over the one-hundred and seventy (170) finite surfaces examined, regardless of the method employed. From the method comparison (Gram-Charlier versus Gauss), with a limited number of measurements (starting from four), the R-squared (R^2The areal roughness values derived from the Gram-Charlier approach exceed 0.99. The precision is confirmed by the method and enhances its reliability.

Meanwhile, the R-squared for the Gaussian approach reaches the same lower limit value (0.99) at the eighth measurement. Table 7 and Table 8 portray the convergence decisions from Equation (10) across all 170 experiments, respectively, from Gram-Charlier and Gaussian methods.

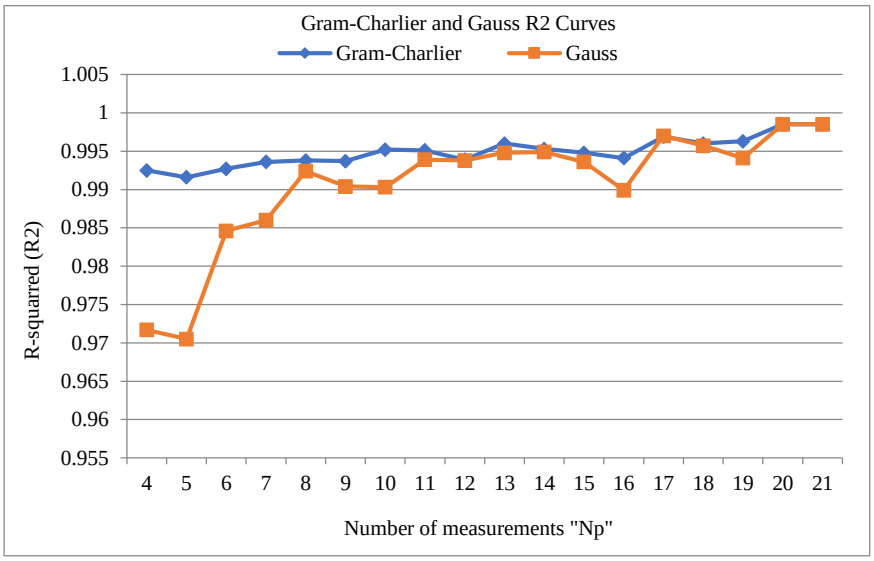

Fig. 7 Coefficient of determination R2 from Gram-Charlier and Gaussian approaches with $N_p \in \langle 4, 5, \ldots, 21 \rangle$ across all finite surfaces

Table 7. Convergence decision from the Gram-Charlier method

N_p	$R^2(N_p)$	$R^2(N_p - 1)$	$CR(N_p)$	Decision
21	0.9986	/	/	/
20	0.9985	0.9986	7.32E-05	Yes
19	0.9964	0.9985	0.0021	Yes
18	0.9961	0.9964	0.0003	Yes
17	0.9968	0.9961	0.0007	Yes
16	0.9941	0.9968	0.0027	Yes
15	0.9948	0.9941	0.0007	Yes
14	0.9954	0.9948	0.0005	Yes
13	0.9960	0.9954	0.0007	Yes
12	0.9940	0.9960	0.0020	Yes
11	0.9951	0.9940	0.0011	Yes
10	0.9953	0.9951	0.0001	Yes
9	0.9937	0.9953	0.0016	Yes
8	0.9938	0.9937	0.0001	Yes
7	0.9936	0.9938	0.0002	Yes
6	0.9927	0.9936	0.0008	Yes
5	0.9916	0.9927	0.0012	Yes
4	0.9925	0.9916	0.0010	Yes

If an algorithm converges faster, it achieves a higher. R^2 value faster with fewer iterations or observations [66]. Table 7 reveals that the Gram-Charlier approach achieved stable R^2 values (CR < 0.01 all over the consecutive N_p).

The observation related to the fewest number of $N_p$permits to expose as from 4 to 6 measurements (blue color in Table 7), the convergence is attained as compared to the Gaussian method, which achieves it in the range from 4 to 8 (the convergence is shown in orange color in Table 8). This represents a 50% reduction in measurement requirements while maintaining equivalent distributional strength ($R^2 > 0.99$ for Gram-Charlier from $N_p = 4$, and $R^2 > 0.99$ for Gaussian from $N_p = 8$, at convergence).

Table 8. Convergence decision from the Gaussian method

N_p	$R^2(N_p)$	$R^2(N_p - 1)$	$CR(N_p)$	Decision
21	0.9986	/	/	/
20	0.9986	0.9986	3.96 E-05	Yes
19	0.9942	0.9986	0.0044	Yes
18	0.9957	0.9942	0.0016	Yes
17	0.9970	0.9957	0.0013	Yes
16	0.9899	0.9970	0.0071	Yes
15	0.9936	0.9899	0.0037	Yes
14	0.9949	0.9936	0.0013	Yes
13	0.9948	0.9949	0.0001	Yes
12	0.9937	0.9948	0.0011	Yes
11	0.9939	0.9937	0.0002	Yes
10	0.9904	0.9939	0.0035	Yes
9	0.9904	0.9904	2.09 E-05	Yes
8	0.9924	0.9904	0.0020	Yes
7	0.9860	0.9924	0.0064	Yes
6	0.9847	0.9860	0.0014	Yes
5	0.9705	0.9847	0.0141	**No**
4	0.9717	0.9705	0.0012	Yes

3.1.4. Distance/Similarity Analysis of Areal Roughness on Machined Replicate Surfaces

After establishing the capability to assess areal roughness via Gram-Charlier developments, it has been beneficial to investigate its behavior on machined replicated surfaces according to the machining conditions. The evaluation of various cutting parameter combinations allows for the observation of the values that can minimize the distance/response, thus achieving perfect replication.

An examination of the measured sets of areal roughness values shows a remarkable similarity among them. The distances or similarities of the eighty-five (85) replicate surfaces, employing Minkowski and Chebyshev distances, alongside the Kullback-Leibler and Jensen-Shannon distance metrics for assessment, are presented in Figure 8. It depicts the fact that as the carbon percentage increases (from 0.10% to 0.30%), the mean distance reduces, showing clearly the impact of the material on the replication process. It depicts the fact that as the carbon percentage increases (from 0.10% to 0.30%), the mean distance reduces, showing clearly the impact of the material on the replication process. More specifically, the Minkowski distance portrays a reduction of mean distance by 29% as the carbon content increases. Chebyshev distance compared to Minkowski's (same family), rather highlights an improvement in the replication possibility.

It is observed that the lowest mean in the Kullback-Leibler distance, but with a very high variability. This proves that in normalizing all the distance metrics, Kullback-Leibler will not be adequate for the replication process. Jensen-Shannon distance is performed identically throughout the materials, which is considered a stationary effect.

This assessment of the replication through the JS distance presents the replication as complicated to implement, taking material into account. Regarding the deviations from all distances to achieve consistent surface replication across all roughness machining conditions, the distance metrics can present interesting values and very low variability in some cases (Minkowski and Shebyshev). A further observation of all the distance metrics values, looking at the contribution of machining conditions in the replication process.

The second-order polynomial regression models were then established from the machining conditions, permitting the representation of their map contribution (Figure 9, Figure 10, and Figure 11) within the values of the experiment. For all four metrics and taking into consideration a cross contribution by pair of machining conditions, the models that perform best regarding family metrics are.

Table 9 highlights the regression models with their respective coefficient of determination, R^2. Ranging from 0.77 to 0.903 and 0.72 to 0.875, Adjusted-R^2 (Adj-R^2) and Predicted-R^2 (Pred-R^2) values, respectively, show interesting fits in the developed models.

From Table 3 (practical meaning) and Table 7 (Adj-R^2 and Pred-R^2), it is noted that the opposite growth of carbon content (increasing) and Adjusted-R^2 values (decreasing) across all distance metrics. The highest predictive accuracy still stands for the AISI1010.

The gap between all Adj-R^2 and Pred-R^2 values, across all metrics and materials, is appreciable considering its low value: 0.20. And so, the criteria above highlight the optimization strategy in the material selection for good repeatability.

As all models meet acceptance criteria, the combination/pair between the Depth of Cut (DoC) and the Spindle Speed (N) appropriately captures interesting features at all levels of combinations: Linear (DoC, N), quadratic (DoC^2, N^2), and two-way interactions (DoC x N).

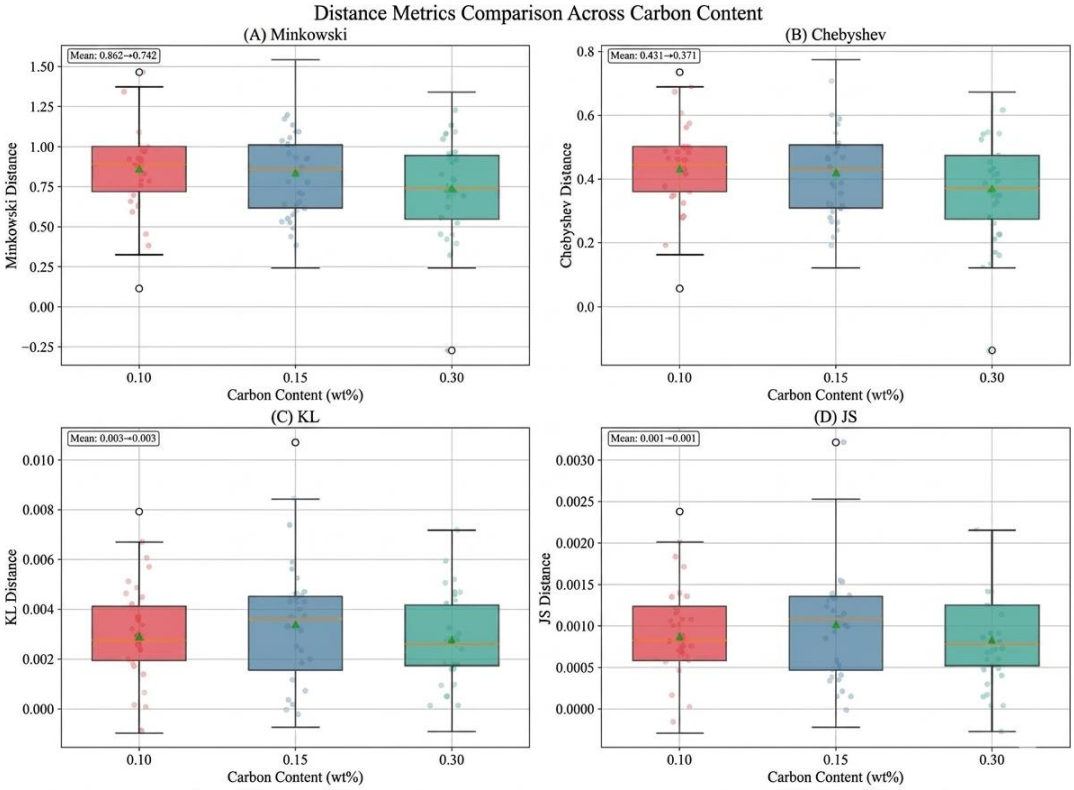

Fig. 8 Distance metrics overview and deviations from materials' perspective

Table 9. Polynomial regression models of distance metrics and performance with materials and machining conditions

Carbon Percent	Family metrics and parameters	Polynomial regression models	R^2	Adj-R^2	Pred-R^2
0.10% (AISI1010 -C10)	Minkowski (DoC, N) at f = 0.0225	$d_{MK(DoC,N)} = 0.983 + 3.08 \times 10^{-5} \cdot DoC - 3.45 \times 10^{-10} \cdot N - 36.29 \cdot DoC^2 + 8.88 \times 10^{-8} \cdot N^2 + 0.0204 \cdot DoC \cdot N + 0.0401 \cdot DoC^2 \cdot N - 1.77 \times 10^{-5} \cdot DoC \cdot N^2$	0.92	0.903	0.875
		$d_{Cheby(DoC,N)} = 0.418 + 1.51 \times 10^{-5} \cdot DoC - 2.001 \times 10^{-10} \cdot N - 21.03 \cdot DoC^2 + 5.14 \times 10^{-8} \cdot N^2 + 0.00845 \cdot DoC \cdot N + 0.0302 \cdot DoC^2 \cdot N - 9.25 \times 10^{-6} \cdot DoC \cdot N^2$	0.88	0.86	0.83
	Jensen-Shannon entropy (N, f) at f = 0.0225	$d_{KL(DoC,N)} = -0.00102 - 2.275 \times 10^{-7} \cdot DoC + 7.60 \times 10^{-9} \cdot N + 0.543 \cdot DoC^2 - 1.33 \times 10^{-9} \cdot N^2 - 0.000123 \cdot DoC \cdot N + 1.77 \times 10^{-7} \cdot N^2 \cdot DoC - 0.00102 \cdot N \cdot DoC^2$	0.91	0.89	0.86
		$d_{JS(DoC,N)} = -0.00102 - 5.903 \times 10^{-8} \cdot DoC + 2.53 \times 10^{-9} \cdot N + 0.181 \cdot DoC^2 - 4.43 \times 10^{-10} \cdot N^2 - 3.14 \times 10^{-5} \cdot DoC \cdot N + 5.01 \times 10^{-8} \cdot N^2 \cdot DoC - 0.000314 \cdot N \cdot DoC^2$	0.89	0.87	0.84
0.15% (AISI1017 – C15)	Minkowski (DoC, N) at f = 0.0225	$d_{MK(DoC,N)} = 0.867 + 2.56 \times 10^{-5} \cdot DoC - 2.89 \times 10^{-10} \cdot N - 30.45 \cdot DoC^2 + 7.45 \times 10^{-8} \cdot N^2 + 0.0171 \cdot DoC \cdot N + 0.0336 \cdot DoC^2 \cdot N - 1.48 \times 10^{-5} \cdot DoC \cdot N^2$	0.88	0.857	0.821

		$\boldsymbol{d_{Cheby(DoC,N)}} = 0.352 + 1.27 \times 10^{-5} \cdot DoC - 1.678 \times 10^{-10} \cdot N - 17.64 \cdot DoC^2 + 4.31 \times 10^{-8} \cdot N^2 + 0.00709 \cdot DoC \cdot N + 0.0253 \cdot DoC^2 \cdot N - 7.76 \times 10^{-6} \cdot DoC \cdot N^2$	0.85	0.82	0.78
	Jensen-Shannon entropy (N, f) at f = 0.0225	$\boldsymbol{d_{KL(DoC,N)}} = -0.00086 - 1.908 \times 10^{-7} \cdot DoC + 6.37 \times 10^{-9} \cdot N + 0.543 \cdot DoC^2 - 1.33 \times 10^{-9} \cdot N^2 - 0.000123 \cdot DoC \cdot N + 1.77 \times 10^{-7} \cdot N^2 \cdot DoC - 0.00102 \cdot N \cdot DoC^2$	0.88	0.86	0.82
		$\boldsymbol{d_{JS(DoC,N)}} = -0.000855 - 4.950 \times 10^{-8} \cdot DoC + 2.12 \times 10^{-9} \cdot N + 0.152 \cdot DoC^2 - 3.71 \times 10^{-10} \cdot N^2 - 2.63 \times 10^{-5} \cdot DoC \cdot N + 4.20 \times 10^{-8} \cdot N^2 \cdot DoC - 0.000263 \cdot N \cdot DoC^2$	0.86	0.84	0.80
0.30% (AISI1038 – C30)	Minkowski (DoC, N) at f = 0.0225	$\boldsymbol{d_{MK(DoC,N)}} = 0.651 + 1.92 \times 10^{-5} \cdot DoC - 2.17 \times 10^{-10} \cdot N - 22.87 \cdot DoC^2 + 5.59 \times 10^{-8} \cdot N^2 + 0.0128 \cdot DoC \cdot N + 0.0252 \cdot DoC^2 \cdot N - 1.11 \times 10^{-5} \cdot DoC \cdot N^2$	0.84	0.841	0.763
		$\boldsymbol{d_{Cheby(DoC,N)}} = 0.264 + 9.52 \times 10^{-5} \cdot DoC - 1.260 \times 10^{-10} \cdot N - 13.23 \cdot DoC^2 + 3.24 \times 10^{-8} \cdot N^2 + 0.00532 \cdot DoC \cdot N + 0.0190 \cdot DoC^2 \cdot N - 5.82 \times 10^{-6} \cdot DoC \cdot N^2$	0.81	0.77	0.72
	Jensen-Shannon entropy (N, f) at f = 0.0225	$\boldsymbol{d_{KL(DoC,N)}} = -0.00064 - 1.433 \times 10^{-7} \cdot DoC + 4.78 \times 10^{-9} \cdot N + 0.342 \cdot DoC^2 - 8.39 \times 10^{-10} \cdot N^2 - 0.0000773 \cdot DoC \cdot N + 1.11 \times 10^{-7} \cdot N^2 \cdot DoC - 0.000642 \cdot N \cdot DoC^2$	0.85	0.82	0.78
		$\boldsymbol{d_{JS(DoC,N)}} = -0.000641 - 3.713 \times 10^{-8} \cdot DoC + 1.59 \times 10^{-9} \cdot N + 0.114 \cdot DoC^2 - 2.78 \times 10^{-10} \cdot N^2 - 1.97 \times 10^{-5} \cdot DoC \cdot N + 3.15 \times 10^{-8} \cdot N^2 \cdot DoC - 0.000197 \cdot N \cdot DoC^2$	0.83	0.80	0.75

Figures 9, 10, and 11 display the response surface for the different materials according to the metrics and machining conditions. For AISI1010, Figure 9 presents a poor appreciation of the replication process due to the low areas covered by the green color at its different shades.

From the metrics viewpoint, it is globally observed that extreme machining conditions (DoC, N) are sensitive. Minkowski and Chebyshev distance metrics identify N = 910 rpm and DoC = 0.2mm as optimal selection, while Kullback-Leibler and Jensen-Shannon prescribe N = 910 rpm and DoC = 0.3mm.

This variation of DoC between 0.2 and 0.3 creates a conflict in the practical selection of machining conditions and does not permit us to conclude in choosing AISI1010 for the replication process. For AISI1017, Figure 10 shows the same conflict as in AISI1010.

For the Minkowski family, N=1280 rpm and DoC=0.3mm, and for the entropy family, N=1280 rpm and DoC=0.2mm. This reduces the discrete choice conflict to a single DoC still between 0.2 and 0.3mm. For AISI1038, Figure 11 totally disconnects the previous organization of Minkowski family metrics. Minkowski distance metrics present their best selection at N = 1280 rpm and DoC = 0.3mm, while Chebyshev is at N = 910 rpm and DoC = 0.1mm. The entropy family remains aligned and meets Chebyshev settings at N and DoC values.

Across all the materials and with consideration of discrete experimental machining conditions, AISI1017 stands as the best choice for the replication process for two main reasons.

Firstly, there is high productivity conferred by the spindle speed (N = 1280 rpm) for all distance metrics. At the same feed (as this is the case here), a high rotational speed permits high productivity.

Secondly, AISI1038 presents diametrically opposed machining conditions' opposition with no adjacent choice in the experimental design space.

Figure 12 underlines the importance of machining conditions taken individually. With the normalized effect size and across all distance metrics, the depth of cut (DoC) is the dominant machining condition for the replication process (effect size > 0.75). The feed rate provides the secondary contribution, and the spindle speed exhibits minimal influence (effect < 0.10 in 8 cases).

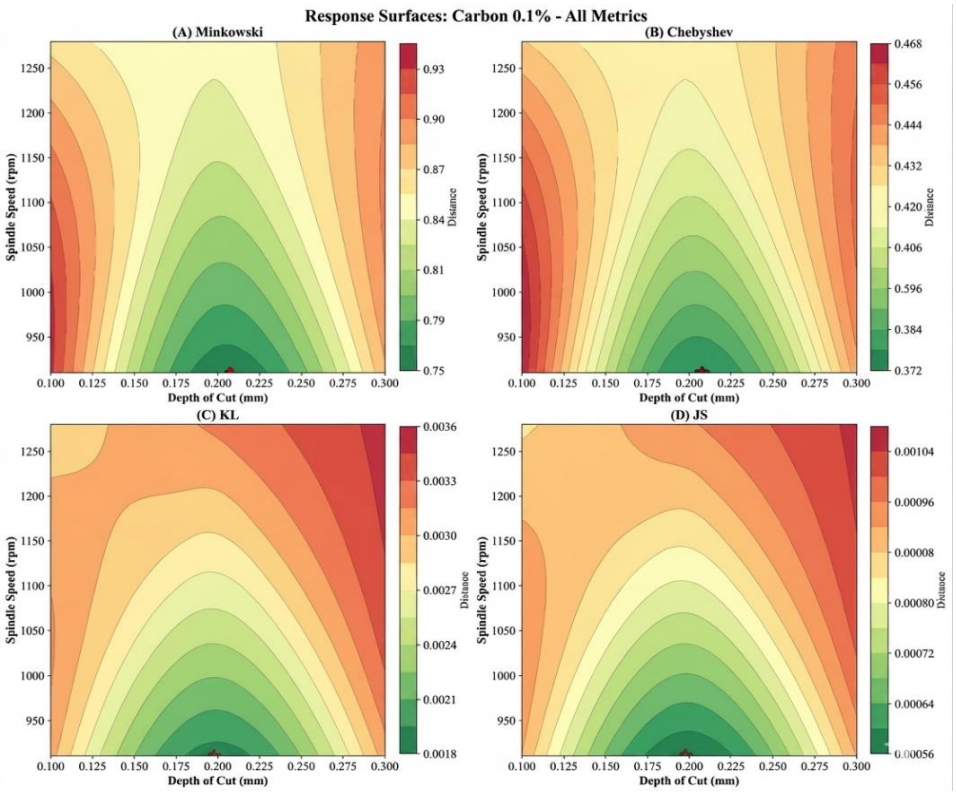

Fig. 9 Response surface for the AISI1010 from the family distance metrics with the DoC and N

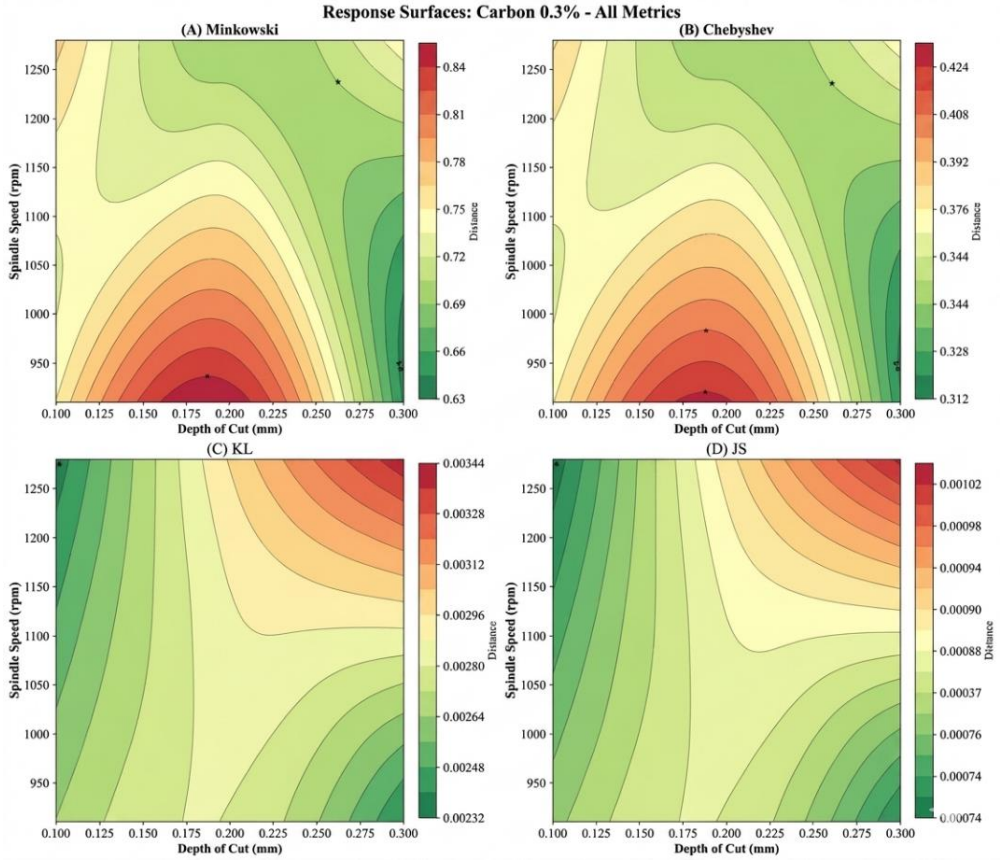

Fig. 10 Response surface for the AISI1017 from the family distance metrics with the DoC and N

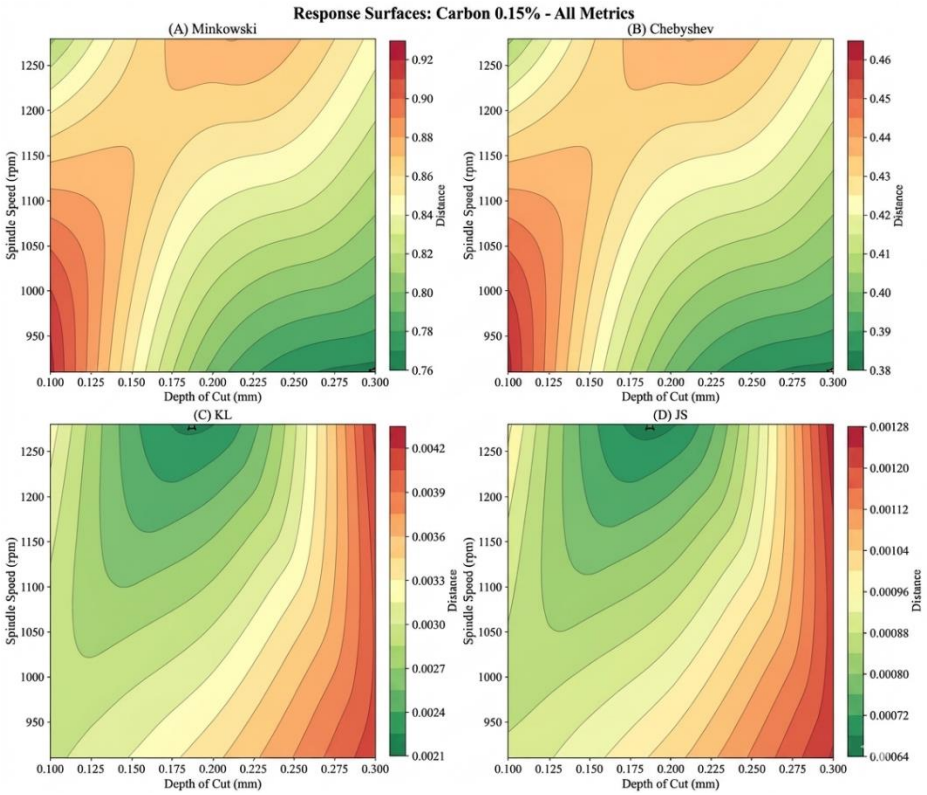

Fig. 11 Response surface for the AISI1038 from the family distance metrics with the DoC and N

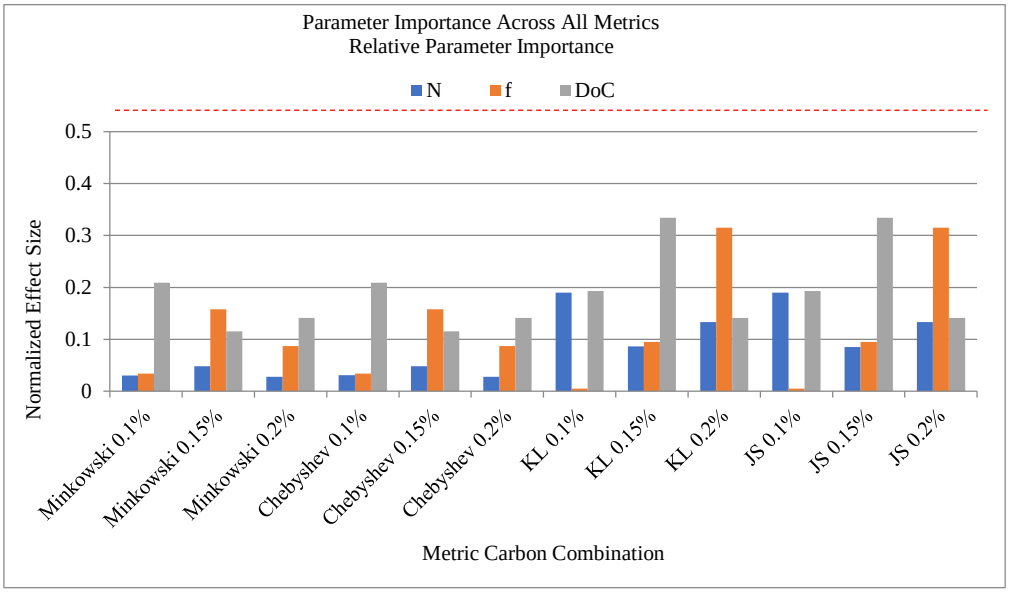

Fig. 12 Machining conditions importance across all metrics

3.2. Discussion

The extraction of a single linear roughness fails to represent the heterogeneity of surfaces adequately. In reality, surfaces frequently display localized variations resulting from manufacturing processes, and a single extraction method is insufficient for determining areal roughness. This assertion was experimentally proven in Figure 7 within this work. [67] underscores the statistical nature of surface roughness, noting that relying on single measurements may lead to a misrepresentation of the surface due to localized irregularities. The results of this work have displayed a considerable range within which the linear roughness values of the same can move and have therefore confirmed the previous statement. Finding a statistical method that faithfully gives the areal

roughness just with a few measurements remains a challenge. The use of the Gram-Charlier series to model linear roughness as a random variable aligns with recent trends in surface metrology that emphasize stochastic approaches. For instance, [51] highlighted the importance of statistical methods in characterizing variables that often follow non-Gaussian distributions. The roughness parameters of the surface texture in milling mostly behave as such due to machining-induced irregularities. The high coefficient of determination ($R^2 > 0.99$) values observed in this study corroborate the findings of [52], who demonstrated that higher-order series expansions (e.g., Gram-Charlier) better capture skewness and kurtosis in experimentation compared to Gaussian models. This suggests that the Gram-Charlier series is a more versatile tool for modeling real-world surface phenomena, particularly in milling processes where tool vibrations and material heterogeneity introduce non-Gaussian features [8].

The proposal of the method to improve areal roughness characterization via contact methods addresses a critical gap in surface metrology. [68] specifies that multiple measurements are necessary to ensure representativeness, particularly for non-uniform surfaces. The standard advocates for traversing different locations and orientations to compute a "mean" value, aligning with industrial quality control practices (ISO, 1996). Industries like aerospace or automotive often mandate multiple measurements for critical components. [69] highlights that high-stakes applications require rigorous metrology to mitigate risks of premature failure. While non-contact optical profilometry (e.g., coherence scanning interferometry) dominates ISO 25178-compliant areal measurements [10], contact profilometers remain widely used in industry due to their cost-effectiveness and simplicity.

The study's success in achieving $R^2 > 0.99$ as from four (04) and throughout the twenty-one (21) linear extractions per surface, supports the argument by [70] that contact methods can remain relevant if augmented with advanced statistical models. The 50% measurement reduction (Np = 4 vs. 6) directly translates to halved inspection time in industrial settings, where stylus setup and acquisition consume approximately one minute per measurement [71]. This efficiency validates fourth-order Gram-Charlier expansion as practical for production environments while maintaining distributional fidelity ($R^2 > 0.99$). This efficiency gain could reduce the time allowed in regressing optical values to contact ones. The relationship between areal roughness and machining parameters (feed, depth of cut, and spindle speed) aligns with foundational studies in machining dynamics. For example, [72] established that feed rate directly influences Peak-To-Valley Roughness (Rz), while [73] showed that depth of cut exacerbates waviness in milled surfaces. The current findings extend these insights by quantifying how parameter combinations affect the statistical distribution of roughness, rather than isolated amplitude parameters. This statistical perspective echoes the work of [73], who Linked Skewness (Rsk) to tool wear mechanisms and Average Roughness (Ra) with the texture parameters. While the method shows promise, its reliance on the coefficient of determination R-squared (R2) as a validation metric warrants caution; the study's focus on milling processes limits its generalizability to other machining operations, namely grinding, EDM, etc, where surface generation mechanisms differ significantly. Future work could integrate machine learning to automate parameter selection and propose the best combination that eases the replication of surfaces.

4. Conclusion

This paper aimed to determine the areal roughness of milled surfaces with the help of linear roughness considered as a random variable. The evaluation of areal roughness has been effected by deriving the Probability Density Function. To validate the estimation of the areal roughness, the coefficient of determination, R-squared (R^2), of the Gram-Charlier series applied over 170 surfaces was compared to standard normal Gaussian density functions across all the surface measurements. The R^2 values assessed from four to twenty-one linear roughness extractions per surface consistently exceeded 0.99 in the Gram-Charlier series, highlighting its relevance in areal roughness evaluation. This analytical approach enabled, with distance/similarity metrics, the establishment of conditions for the replication of surfaces, specifically in relation to machining parameters such as feed, depth of cut, and spindle speed. The depth of cut has been revealed as the most important, and the carbon steel with 0.15% (AISI1017) has shown the best carbon content for the replication process. The findings presented provide a groundwork for improving the characterization of the areal roughness via contact methods, and propose a practical bridge to the passage of the specifications of norm ISO 4287 to ISO 25178, irrespective of surface phenomena. Thus, it is expected that the mechanisms governing the surface will perform optimally based on their defined parameters. Furthermore, future research endeavors will focus on enhancing and automating the assessment of the areal roughness in machined surfaces.

Conflicts of Interest

The authors declare there are no conflicts of interest regarding the publication of this paper.

Funding Statement

The authors declare that the research and publication of the article received no funding from any institution or organization except the authors' self-contribution.

Acknowledgments

We appreciate the collaborative efforts of our colleague Mpacko Charles, Head of the Mechanical Engineering Department, University Institute of Technology, University of Douala.

References

[1] Rüstem Binali et al., "Machinability Investigations Based on Tool Wear, Surface Roughness, Cutting Temperature, Chip Morphology and Material Removal Rate during Dry and MQL-Assisted Milling of Nimax Mold Steel," *Lubricants*, vol. 11, no. 3, pp. 1-14, 2023. [CrossRef] [Google Scholar] [Publisher Link]

[2] Praveen Kumar Gandla et al., "Evaluation of Surface Roughness in Incremental Forming Using Image Processing-Based Methods," Measurement, vol. 164, 2020. [CrossRef] [Google Scholar] [Publisher Link]

[3] Baofeng He, Siyuan Ding, and Zhaoyao Shi, "A Comparison between Profile and Areal Surface Roughness Parameters," *Metrology and Measurement Systems*, vol. 28, no. 3, pp. 413-438, 2021. [CrossRef] [Google Scholar] [Publisher Link]

[4] J. Schmidt et al., "Comparison of Areal and Profile Surface Measurement Methods for Evaluating Surface Properties of Machined Components," *Procedia CIRP*, vol. 102, pp. 459-464, 2021. [CrossRef] [Google Scholar] [Publisher Link]

[5] Alain Cornet, and Jean-Paul Deville, *Surface Physics and Engineering*, EDP Sciences, 1998. [Google Scholar] [Publisher Link]

[6] Shi Hyoung Ryu, Deok Ki Choi, and Chong Nam Chu, "Roughness and Texture Generation on End Milled Surfaces," *International Journal of Machine Tools and Manufacture*, vol. 46, no. 3-4, pp. 404-412, 2006. [CrossRef] [Google Scholar] [Publisher Link]

[7] V.F. Bez''yazychnyi, and A.N. Sutyagin, "Influence of Vibration on Surface Roughness in Turning," *Russian Engineering Research*, vol. 39, no. 7, pp. 612-616, 2019. [CrossRef] [Google Scholar] [Publisher Link]

[8] D.D. Trung, "Influence of Cutting Parameters on Surface Roughness during Milling AISI 1045 Steel," *Tribology in Industry*, vol. 42, no. 4, pp. 658-665, 2020. [CrossRef] [Google Scholar] [Publisher Link]

[9] John Henry Navarro-Devia et al., "Chatter Detection in Milling Processes - A Review on Signal Processing and Condition Classification," *The International Journal of Advanced Manufacturing Technology*, vol. 125, no. 9-10, pp. 3943-3980, 2023. [CrossRef] [Google Scholar] [Publisher Link]

[10] Richard Leach, *Characterisation of Areal Surface Texture*, 1st ed., Springer Berlin, Heidelberg, 2013. [CrossRef] [Google Scholar] [Publisher Link]

[11] Vladimir Lyukshin, Dmitry Shatko, and Pavel Strelnikov, "Methods and Approaches to the Surface Roughness Assessment," *Materials Today: Proceedings*, vol. 38, pp. 1441-1444, 2020. [CrossRef] [Google Scholar] [Publisher Link]

[12] Shilpa Karegoudra, and Vamsidhar Yendapalli, "A Systematic Review on Non-Contact Methods to Estimate the Surface Roughness," *Materials Today: Proceedings*, vol. 100, pp. 75-92, 2024. [CrossRef] [Google Scholar] [Publisher Link]

[13] Dana Kubátová, "Problems of Surface Roughness Measurement with a Focus on the Scanned Points," *Proceedings of the 29th DAAAM International Symposium*, Vienna, Austria, pp. 1256-1265, 2018. [CrossRef] [Google Scholar] [Publisher Link]

[14] Szeréna-Krisztina Fecske et al., "Interdependence of Amplitude Roughness Parameters on Rough Gaussian Surfaces," *Tribology Letters*, vol. 68, no. 43, 2020. [CrossRef] [Google Scholar] [Publisher Link]

[15] Juraj Ružbarský, "The Difficulty of Measuring the Roughness of Glossy Surfaces Using the Triangulation Principle," *Applied Sciences*, vol. 13, no. 8, pp. 1-14, 2023. [CrossRef] [Google Scholar] [Publisher Link]

[16] G. Farkas, and Á. Drégelyi-Kiss, "Measurement Uncertainty of Surface Roughness Measurement," *IOP Conference Series: Materials Science and Engineering, XXIII International Conference on Manufacturing*, Kecskemét, Hungary, vol. 448, 2018. [CrossRef] [Google Scholar] [Publisher Link]

[17] Enhui Lu et al., "Designing Indices to Measure Surface Roughness Based on the Color Distribution Statistical Matrix (CDSM)," *Tribology International*, vol. 122, pp. 96-107, 2018. [CrossRef] [Google Scholar] [Publisher Link]

[18] Donna L. Mohr, William J. Wilson, and Rudolf J. Freund, *Chapter 2 - Probability and Sampling Distributions*, Statistical Methods, 4th ed., Academic Press, pp. 65-122, 2022. [CrossRef] [Publisher Link]

[19] Yves Brunet-Moret, Distribution Functions in Limited Development, ORSTOM Notebooks, Hydrology Series, 1971. [Online]. Available: https://horizon.documentation.ird.fr/exl-doc/pleins_textes/pleins_textes_4/hydrologie/14871.pdf

[20] Chris Tsokos, and Rebecca Wooten, *The Joy of Finite Mathematics: The Language and Art of Math*, Academic Press, 2016. [CrossRef] [Google Scholar] [Publisher Link]

[21] Tieyuan Shen, and Yiheng Xiang, "Optimization of Probability Density Functions Applicable for Hourly Rainfall," *Atmosphere*, vol. 14, no. 7, pp. 1-23, 2023. [CrossRef] [Google Scholar] [Publisher Link]

[22] Harald Cramér, *Mathematical Methods of Statistics*, Princeton University Press, 1999. [Google Scholar] [Publisher Link]

[23] William Feller, *An Introduction to Probability Theory and its Applications, Volume 2*, 2nd ed., Wiley, 1971. [Google Scholar] [Publisher Link]

[24] Singiresu S. Rao, *Engineering Optimization: Theory and Practice*, 4th ed., Wiley, 2019. [CrossRef] [Google Scholar] [Publisher Link]

[25] S. Blinnikov, and R. Moessner, "Expansions for Nearly Gaussian Distributions," *Astronomy and Astrophysics Supplement Series*, vol. 130, no. 1, pp. 193-205, 1998. [CrossRef] [Google Scholar] [Publisher Link]

[26] Junye Ma, and Lin Li, "Literature Review on Engineering Surface Modeling," *MethodsX*, Vol. 10, 2023. [CrossRef] [Google Scholar] [Publisher Link]

[27] Tobias Grimm et al., "Surface Analysis in Additive Manufacturing: A Systematic Literature Review Regarding Powder Bed Fusion Processes," *Surface Topography: Metrology and Properties*, vol. 13, no. 1, pp. 1-36, 2025. [CrossRef] [Google Scholar] [Publisher Link]

[28] Carsten Engler et al., "New Method for Assessing the Repeatability of the Measuring System for Roughness Measurements," *International Journal of Metrology and Quality Engineering (IJMQE)*, vol. 155, pp. 1-15, 2024. [CrossRef] [Google Scholar] [Publisher Link]

[29] Eric Jondeau, and Michael Rockinger, "Gram-Charlier Densities," *Journal of Economic Dynamics and Control*, vol. 25, no. 10, pp. 1457-1483, 2001. [CrossRef] [Google Scholar] [Publisher Link]

[30] Armando Pelliccioni, "The Gram-Charlier Method to Evaluate the Probability Density Function in Monodimensional Case," *Nuovo Cimento-Italian Physical Society Section C*, pp. 432-452, 1996. [Google Scholar]

[31] Maria Grazia Zoia, Gianmarco Vacca, and Laura Barbieri, "Modeling Multivariate Financial Series and Computing Risk Measures via Gram-Charlier-Like Expansions," *Risks*, vol. 8, no. 4, pp. 1-21, 2020. [CrossRef] [Google Scholar] [Publisher Link]

[32] Ángel León, and Trino-Manuel Ñíguez, "The Transformed Gram Charlier Distribution: Parametric Properties and Financial Risk Applications," *Journal of Empirical Finance*, vol. 63, pp. 323-349, 2021. [CrossRef] [Google Scholar] [Publisher Link]

[33] A. Pelliccioni A, and M. Angeloni, "A New Formulation of the Gram-Charlier Method: Performance for Fitting Non-Normal Distribution," *Nuovo Cimento-Italian Physical Society Section C*, vol. 30, no, 4, pp. 381-394, 2007. [Google Scholar]

[34] Wei Wang, Naoki Ikegaya, and Tsubasa Okaze, "Comparing Weibull Distribution Method and Gram-Charlier Series Method within the Context of Estimating Low-Occurrence Strong Wind Speed of Idealized Building Cases," *Journal of Wind Engineering and Industrial Aerodynamics*, vol. 236, 2023. [CrossRef] [Google Scholar] [Publisher Link]

[35] Grzegorz Tyl et al., "Population Balance Approach to Model Ostwald Ripening of Silica Using Gram-Charlier Series Expansion-Based Closure," *Chemical Engineering Research and Design*, vol. 159, pp. 491-504, 2020. [CrossRef] [Google Scholar] [Publisher Link]

[36] William Palin Elderton, *Frequency Curves and Correlation*, 4th ed., Cambridge University Press, 2011. [Google Scholar] [Publisher Link]

[37] Samuel Kotz, *Distribution in Statistics: Continuous Univariate Distributions*, John Wiley & Sons, 1970. [Google Scholar]

[38] Alan Stuart, and Keith Ord, *Kendall's Advanced Theory of Statistics, Volume 1, Distribution Theory*, 6th Ed., John Wiley & Sons, 2010. [Google Scholar] [Publisher Link]

[39] R.A. Fisher, *Statistical Methods for Research Workers*, Breakthroughs in Statistics, Springer, New York, NY, pp. 66-70, 1992. [CrossRef] [Google Scholar] [Publisher Link]

[40] Solomon Kullback, and Richard A. Leibler, "On Information and Sufficiency," *The Annals of Mathematical Statistics*, vol. 22, no. 1, pp. 79-86, 1951. [Google Scholar] [Publisher Link]

[41] L.N. Vaserstein, "Markov Processes Over Denumerable Products of Spaces Describing Large Systems of Automata," *Problems of Information Transfer*, vol. 5, no. 3, pp. 64-73, 1969. [Google Scholar] [Publisher Link]

[42] Alison L. Gibbs, and Francis Edward Su, "On Choosing and Bounding Probability Metrics," *International Statistical Review*, vol. 70, no. 3, pp. 419-435, 2002. [CrossRef] [Google Scholar] [Publisher Link]

[43] Jie Yu et al., "A New Study on Distance Metrics as Similarity Measurement," *2006 IEEE International Conference on Multimedia and Expo*, Toronto, ON, Canada, pp. 533-536, 2006. [CrossRef] [Google Scholar] [Publisher Link]

[44] Sung-Hyuk Cha, "Comprehensive Survey on Distance/Similarity Measures between Probability Density Functions," *International Journal of Mathematical models and Methods in Applied Sciences*, vol. 1, no. 4, pp. 300-307, 2007. [CrossRef] [Google Scholar] [Publisher Link]

[45] M-J. Lesot, M. Rifqi, and H. Benhadda, "Similarity Measures for Binary and Numerical Data: A Survey," *International Journal of Knowledge Engineering and Soft Data Paradigms*, vol. 1, no. 1, pp. 63-84, 2008. [CrossRef] [Google Scholar] [Publisher Link]

[46] Seung-Seok Choi, Sung-Hyuk Cha, and Charles C. Tappert, "A Survey of Binary Similarity and Distance Measures," *Journal of Systemics, Cybernetics and Informatics*, vol. 8, no. 1, pp. 43-48, 2010. [Google Scholar] [Publisher Link]

[47] Shaker K. Ali, Zahoor M. Aydam, and Biadaa M. Rashed, "Similarity Metrics for Classification: A Review," *IOP Conference Series: Materials Science and Engineering: 2nd International Scientific Conference of Al-Ayen University (ISCAU-2020)*, Thi-Qar, Iraq, vol. 928, pp. 1-18, 2020. [CrossRef] [Google Scholar] [Publisher Link]

[48] Shuyuan Yang et al., "Progressive Neighbours' Pursuit for Radar Images Classification," *Applied Soft Computing*, vol. 109, 2021. [CrossRef] [Google Scholar] [Publisher Link]

[49] Fischer Black, and Myron Scholes, "The Pricing of Options and Corporate Liabilities," *Journal of Political Economy*, vol. 81, no. 3, pp. 637-654, 1973. [CrossRef] [Google Scholar] [Publisher Link]

[50] R.E. Kalman, "A New Approach to Linear Filtering and Prediction Problems," *Journal of Fluids Engineering*, vol. 82, no. 1, pp. 35-45, 1960. [CrossRef] [Google Scholar] [Publisher Link]

[51] Carl Edward Rasmussen, and Christopher K.I. Williams, *Gaussian Processes for Machine Learning*, MIT Press, 2005. [CrossRef] [Google Scholar] [Publisher Link]

[52] Douglas A. Reynolds, Thomas F. Quatieri, and Robert B. Dunn, "Speaker Verification Using Adapted Gaussian Mixture Models," *Digital Signal Processing*, vol. 10, no. 1-3, pp. 19-41, 2000. [CrossRef] [Google Scholar] [Publisher Link]

[53] HáKon Gudbjartsson, and Samuel Patz, "The Rician Distribution of Noisy MRI Data," *Magnetic Resonance in Medicine*, vol. 34, no. 6, pp. 910-914, 1995. [CrossRef] [Google Scholar] [Publisher Link]

[54] R. Lyman Ott, and Michael T. Longnecker, *An Introduction to Statistical Methods and Data Analysis*, 7th ed., Brooks/Cole, Cengage Learning, 2010. [Google Scholar] [Publisher Link]

[55] Wei Wang, Koki Seta, and Naoki Ikegaya, "Modelling Probability Density Functions based on the Gram-Charlier Series with Higher-Order Statistics: Theoretical Derivation and Application," *Journal of Wind Engineering and Industrial Aerodynamics*, vol. 231, 2022. [CrossRef] [Google Scholar] [Publisher Link]

[56] Jacques Goupy, *Introduction to Experimental Design*, 5th ed., Dunod, 2017. [Publisher Link]

[57] P. Dagnelie, "Statistical Theory and Methods (vol. 2). Gembloux Agricultural Press, *Variability of the Rainfall Regime of Non-Sahelian West Africa*, 1975. [Google Scholar]

[58] Wei Lin, and Jin E. Zhang, "The Valid Regions of Gram-Charlier Densities with High Order Cumulants," *Journal of Computational and Applied Mathematics*, vol. 407, 2022. [CrossRef] [Google Scholar] [Publisher Link]

[59] Mário N. Berberan-Santos, "Expressing a Probability Density Function in Terms of Another PDF: A Generalized Gram-Charlier Expansion," *Journal of Mathematical Chemistry*, vol. 42, no. 3, pp. 585-594, 2006. [CrossRef] [Google Scholar] [Publisher Link]

[60] D.E. Barton, and K.E. Dennis, "The Conditions under Which Gram-Charlier and Edgeworth Curves are Positive Definite and Unimodal," *Biometrika*, vol. 39, no. 3-4, pp. 425-427, 1952. [CrossRef] [Google Scholar] [Publisher Link]

[61] Jean-Pierre Chateau, and Daniel Dufresne, "Gram-Charlier Processes and Equity-Indexed Annuities," *Centre for Actuarial Studies, University of Melbourne, Working Paper 227*, 2012. [Google Scholar]

[62] Oh Kang Kwon, "Analytic Expressions for the Positive Definite and Unimodal Regions of Gram-Charlier Series," *Communications in Statistics - Theory and Methods*, vol. 51, no. 15, pp. 5064-5084, 2022. [CrossRef] [Google Scholar] [Publisher Link]

[63] Sai Lotfi et al., "The Effect of High-Speed Milling on Surface Roughness of 42CrMo4 Hardened Steel Using a Ball Nose End-Mill Cutter," *International Conference Design and Modeling of Mechanical Systems*, Hammamet, Tunisia, vol. 1, pp. 375-381, 2019. [CrossRef] [Google Scholar] [Publisher Link]

[64] Davide Chicco, Matthijs J. Warrens, and Giuseppe Jurman, "The Coefficient of Determination R-Squared is more Informative than SMAPE, MAE, MAPE, MSE and RMSE in Regression Analysis Evaluation," *PeerJ Computer Science*, vol. 7, pp. 1-24, 2021. [CrossRef] [Google Scholar] [Publisher Link]

[65] V.B. Bokov, "Surface Roughness in Final Turning: Development of an Adequate Empirical Model," *Russian Engineering Research*, vol. 36, no. 7, pp. 559-564, 2016. [CrossRef] [Google Scholar] [Publisher Link]

[66] David J. Whitehouse, *Handbook of Surface Metrology*, 1st ed., CRC Press, 1994. [CrossRef] [Google Scholar] [Publisher Link]

[67] ISO 4288:1996, Geometrical Product Specifications (GPS) - Surface Texture: Profile Method - Rules and Procedures for the Assessment of Surface Texture, ISO, 1996. [Online]. Available: https://www.iso.org/standard/2096.html

[68] Stanislaw Raczynski, *Chapter Eleven - Uncertain Future: A Trip*, Reachable Sets of Dynamic Systems, Academic Press, 2023. [CrossRef] [Google Scholar] [Publisher Link]

[69] Bharat Bhushan, *Principles and Applications of Tribology*, John Wiley & Sons, 2013. [CrossRef] [Google Scholar] [Publisher Link]

[70] Claudiu L. Giusca, Richard K. Leach, and Frank Helery, "Calibration of the Scales of Areal Surface Topography Measuring Instruments: Part 2 – Amplification Coefficient, Linearity and Squareness," *Measurement Science and Technology*, vol. 23, no. 6, 2012. [CrossRef] [Google Scholar] [Publisher Link]

[71] Tzu-Liang Tseng, Udayvarun Konada, and Yongjin Kwon, "A Novel Approach to Predict Surface Roughness in Machining Operations using Fuzzy Set Theory," *Journal of Computational Design and Engineering*, vol. 3, no. 1, pp. 1-13, 2016. [CrossRef] [Google Scholar] [Publisher Link]

[72] A.I. Germashev et al., "Influence of the Cut Axial Depth on Surface Roughness at High-Speed Milling of Thin-Walled Workpieces," Science and Technology, vol. 20, no. 2, pp. 127-131, 2021. [CrossRef] [Google Scholar] [Publisher Link]

[73] Pradeep L. Menezes, Kishore, Satish V. Kailas, "Influence of Roughness Parameters on Coefficient of Friction under Lubricated Conditions," Sadhana, vol. 33, no. 3, pp. 181-190, 2008. [CrossRef] [Google Scholar] [Publisher Link]

Appendix

Table 4. (start) Matrix of the linear roughness values with rotational speed (N) in rpm, feed rate (f) in mm/tooth, Depth of Cut (DoC) in mm, Tool life (Tl) in s.

F_{sk}	%C	N	f	DoC	Tl	$r_{a,1}$	$r_{a,2}$	$r_{a,3}$	$r_{a,4}$	$r_{a,5}$	$r_{a,6}$	$r_{a,7}$	$r_{a,8}$	$r_{a,9}$	$r_{a,10}$	$r_{a,11}$
F_{s1}	0.1	1280	29	0.1	69.3	0.206	0.316	0.243	0.264	0.187	0.245	0.332	0.295	0.301	0.241	0.301
F_{s2}	0.1	1280	29	0.1	138.5	0.188	0.298	0.349	0.169	0.316	0.331	0.354	0.294	0.294	0.277	0.369
F_{s6}	0.1	1280	29	0.1	75	0.145	0.291	0.237	0.148	0.281	0.358	0.292	0.236	0.233	0.702	0.704
F_{s7}	0.1	1280	29	0.1	149	0.36	0.324	0.599	0.448	0.361	0.34	0.326	0.35	0.319	0.715	0.63
F_{s10}	0.1	1280	29	0.1	78	1.033	1.094	1.476	1.354	1.018	0.943	1.061	1.076	1.103	0.94	0.96
F_{s11}	0.1	1280	29	0.2	156	1.304	1.282	1.452	1.895	1.953	1.431	1.282	1.487	1.326	1.603	1.702
F_{s14}	0.1	910	16	0.1	120	2.41	2.089	2.048	1.94	1.977	1.873	1.872	2.053	1.89	1.766	1.732
F_{s15}	0.1	1280	29	0.2	240	1.982	2.045	1.617	1.632	1.718	1.678	1.69	1.789	1.794	2.1	1.972
F_{s16}	0.1	1280	29	0.2	91	1.469	1.416	1.492	1.598	1.382	1.254	1.27	1.2	1.141	0.956	1.27
F_{s18}	0.1	910	16	0.2	135	2.53	2.069	2.009	2.056	1.893	1.858	1.875	1.592	1.689	1.681	1.68
F_{s19}	0.1	1280	29	0.2	269	1.842	1.84	1.847	1.857	1.889	2.045	1.9	1.884	1.902	1.676	1.675
F_{s46}	0.3	1280	29	0.1	80	0.428	0.762	0.496	0.526	0.578	0.732	0.367	0.395	0.441	0.417	0.374
F_{s47}	0.3	1280	29	0.1	160	0.583	0.37	0.421	0.439	0.378	0.385	0.746	0.346	0.361	0.363	0.345
F_{s92}	0.3	910	16	0.2	292.9	1.228	1.213	1.087	1.215	1.218	1.32	1.422	1.278	1.287	1.278	1.277
F_{s100}	0.15	910	16	0.3	154.1	2.092	1.723	1.871	2.93	1.401	1.456	1.319	1.448	1.376	1.293	1.237
F_{s141}	0.15	910	16	0.1	184.2	2.297	1.84	1.75	1.703	1.704	2.122	1.599	1.533	1.412	2.16	1.606
F_{s161}	0.15	910	16	0.3	106.4	1.509	1.668	1.537	1.471	1.438	1.377	1.432	1.514	1.358	1.543	1.438
F_{s169}	0.15	910	16	0.3	432	1.707	2.044	1.806	1.539	1.481	1.908	1.931	1.813	1.771	1.874	1.745

Table 5. (end) Matrix of the linear roughness values

F_{sk}	%C	N	f	DoC	Tl	$r_{a,12}$	$r_{a,13}$	$r_{a,14}$	$r_{a,15}$	$r_{a,16}$	$r_{a,17}$	$r_{a,18}$	$r_{a,19}$	$r_{a,20}$	$r_{a,21}$	$r_{a,22}$	$r_{a,23}$
F_{s1}	0.1	1280	29	0.1	69.3	0.237	0.197	0.17	0.206	0.261	0.226	0.224	0.173	0.202	0.26	0.505	0.395
F_{s2}	0.1	1280	29	0.1	138.5	0.243	0.157	0.175	0.185	0.267	0.217	0.233	0.269	0.463	0.452	0.516	0.553
F_{s6}	0.1	1280	29	0.1	75	0.606	0.63	0.605	0.52	0.542	0.529	0.462	0.492	0.429	0.474	0.461	0.475
F_{s7}	0.1	1280	29	0.1	149	0.732	0.831	0.686	0.63	0.632	0.552	0.579	0.592	0.633	0.533	0.059	0.596
F_{s10}	0.1	1280	29	0.1	78	0.977	0.888	0.896	0.899	0.807	0.818	0.826	0.786	0.688	0.983	0.557	1.112
F_{s11}	0.1	1280	29	0.2	156	1.745	1.892	1.727	1.732	1.411	0.843	0.809	1.139	0.588	0.549	0.511	1.097
F_{s14}	0.1	910	16	0.1	120	1.835	1.777	1.698	1.687	1.835	1.774	1.488	1.422	1.372	1.315	1.221	1.16
F_{s15}	0.1	1280	29	0.2	240	1.517	1.674	1.778	1.652	1.574	1.575	1.323	1.527	1.428	1.327	1.28	1.346
F_{s16}	0.1	1280	29	0.2	90.3	1.787	1.473	0.976	1.457	1.043	1.134	0.805	1.088	0.733	0.644	0.874	1.104
F_{s18}	0.1	910	16	0.2	135	1.638	1.721	1.687	1.594	1.52	1.561	1.608	1.576	1.594	1.437	1.509	1.315

F_{s19}	0.1	1280	29	0.2	269	1.786	1.762	1.713	1.942	1.802	1.796	1.706	1.772	1.822	1.801	1.677	1.498
F_{s46}	0.3	1280	29	0.1	80	0.375	0.403	0.385	0.39	0.388	0.37	0.396	0.478	0.464	0.476	0.288	0.347
F_{s47}	0.3	1280	29	0.1	158.2	0.497	0.354	0.897	0.67	0.283	0.366	0.796	0.254	0.204	0.324	0.297	0.26
F_{s92}	0.3	910	16	0.2	292.9	1.354	1.314	1.186	1.176	1.089	1.119	1.029	0.955	1.051	1.059	0.987	1.079
F_{s100}	0.15	910	16	0.3	154.1	1.176	1.369	1.226	1.206	1.252	1.246	1.243	1.147	0.978	1.181	1.147	1.196
F_{s141}	0.15	910	16	0.1	184.2	1.608	1.771	1.627	1.713	1.643	1.709	1.656	1.603	1.627	1.626	1.732	1.729
F_{s161}	0.15	910	16	0.3	106.4	1.456	1.58	1.683	1.841	1.706	1.592	1.361	1.5	1.35	1.593	1.434	1.12
F_{s169}	0.15	910	16	0.3	432	1.501	1.236	1.459	1.491	1.454	1.467	1.485	1.021	1.088	1.08	1.12	0.895